FINAL SCIENTIFIC/TECHNICAL REPORT

Submitted To:

U.S. Department of Energy

Office of Fossil Energy

Advanced Combustion Systems

Award #DE-FE0025193

Project Title:

Integrated Flue Gas Purification and Latent Heat Recovery for Pressurized Oxy-Combustion

Principal Investigator:

Richard L. Axelbaum, Professor

(314) 935-7560

axelbaum@wustl.edu

Submission Date: February 11, 2019

DUNS Number 068552207

Recipient Organization:

Washington University

One Brookings Dr.

Saint Louis, MO 63130

Project/Grant Period: 9/1/2015 – 8/31/2018

Final Scientific/Technical Report

Contributing Authors

David Stokie[a]
Piyush Verma[a]
Benjamin Kumfer[a]
Yujia Min[a]
Yaguang Zhu[a]
Young-Shin Jun[a]
Grigoriy Yablonsky[a]
A.K. Suresh[b]
Richard L. Axelbaum[a]

a Dept. Energy, Environmental & Chemical Engineering Washington University, St. Louis, USA
b Dept. Chemical Engineering, Indian Institute of Technology Bombay, India

TABLE OF CONTENTS

LIST OF FIGURES

LIST OF TABLES

1. Executive Summary

Pressurized oxy-combustion has been identified by DOE as a transformational technology for coal power with carbon capture due to the advantages that are realized when the combustion process is pressurized. The staged pressurized oxy-combustion (SPOC) process is particularly attractive as the efficiency of the process is almost 6 percentage points greater than that of first generation oxy-combustion. A critical component of the SPOC process, and potentially other pressurized combustion processes, is the Direct Contact Cooler (DCC) where the latent heat of the flue gas moisture is recovery to improve plant efficiency while simultaneously removing SOx and NOx from the flue gas, so that the FGD and de-NOx processes can be eliminated, and the cost of electricity minimized.

The objective of this R&D effort was to advance the TRL of the DCC technology, which included performance testing at a 100 kW scale to validate the process and obtain key engineering data for scale-up. A collateral objective was to study the gas- and liquid-phase kinetics, and the development of a systematic chemical mechanism validated by experimental data. Experiments in a bench-scale stirred reactor provided an updated understanding of the liquid chemistry and the effects of temperature and pH. This information was used to develop a reduced reaction mechanism, which was subsequently incorporated in an ASPEN-based process model, to allow for evaluation of the DCC at full scale.

A small-pilot DCC column was designed, constructed and tested using simulated flue gas at the pressurized oxy-combustion test facility at Washington University in St. Louis. In the majority of tests, the SO_2 capture approached 100%, making the NO_x capture the primary metric of capture efficiency. An NO_x capture efficiency of 90% was achieved when the gas residence time was 95 seconds, demonstrating that high capture rates can be attained with reasonable reactor size. At higher temperatures (up to 200°C inlet gas temperature) the total NOx scrubbing efficiency was reduced by approximately 10% (compared to room temp.) and this was attributed to a reduced NO oxidation rate. A significant amount of SO_2 was present in the gas outlet (10%) only when the temperature was high and the N:S ratio was low ($N/S < 1$), which highlights the necessity of controlling the NOx concentration in the flue gas for complete sulfur scrubbing.

After incorporated our optimized chemical mechanism into an ASPEN process model, various full-scale configurations of the DCC were evaluate, and the results indicate that the proposed DCC can accomplish its intended goals at full scale and at a modest size. Thus, the results of this project indicate that the DCC is a promising technology for recovery of the latent heat of the moisture in the flue gas while simultaneously scrubbing the nitrogen and sulfur oxides, thus enabling pressurized oxy-combustion, in general, and the SPOC process, in particular.

2. Background

2.1 Staged Pressurized Oxy-Combustion

Carbon capture, utilization and sequestration (CCUS) provides a path for continuing to benefit from fossil fuel combustion for reliable power generation, while drastically reducing atmospheric CO_2 emissions. Oxy-fuel combustion is one such technology that has received considerable attention. By combusting fuel in oxygen, instead of air, the outlet flue gas is predominantly CO_2 (after moisture removal), with minimal amounts of O_2 and N_2, resulting in an outlet stream suitable for carbon utilization or storage. The costs associated with *first-generation* oxy-combustion technology are currently prohibitive. First-generation technologies consist of burning coal at nearly atmospheric pressure with oxygen and a large volume of recycled flue gas. The recycled flue gas is used to control flame temperature and heat transfer in the boiler, yielding conditions similar to those of traditional air-fired boilers.

The high cost of electricity for oxy-combustion systems largely stems from production of oxygen in the Air Separation Unit (ASU), and from the compression and purification of carbon dioxide in preparation for geo-sequestration or EOR. These additional processes increase capital equipment costs and lead to a significant loss in power plant efficiency. Other technologies for carbon capture, e.g., IGCC and post-combustion capture, also suffer with respect to low efficiency and high cost. For these reasons, the U.S. Department of Energy (DOE) has set a goal of developing technologies that lead to 90% capture of carbon dioxide, with an increased cost of electricity of no more than 35%, as compared to a similar plant without carbon capture.

The fact that CCUS requires high-pressure CO_2 and that the energy to compress O_2 is comparable to that needed to compress the corresponding CO_2, enables the boilers to be operated under pressure during oxy-combustion. *Pressurized* oxy-combustion has been identified by DOE as a transformational technology for coal power due to the advantages that are obtained when the combustion process is pressurized, and the Staged Pressurized Oxy-Combustion (SPOC) process represents a step change in improving the cost and efficiency for pressurized oxy-combustion. The primary benefits of the SPOC process include: (1) the

latent heat of moisture in the flue gas is recovered (to improve efficiency), while simultaneously removing almost all the SO_X, and much of the NO_X and mercury in the flue gas; (2) modular boiler construction is possible, which will reduce construction time and costs; (3) minimal flue gas recirculation (FGR) is needed to control wall heat flux, which nearly eliminates the pumping power associated with FGR, minimizes flue-gas volume, increases efficiency and reduces component size and costs; (4) radiative heat transfer is maximized, which improves efficiency and minimizes heat transfer surface requirements and hence cost; and (5) flexible operation is inherent, resulting from the staged, modular design, thereby allowing for improved plant ramping rates and turndown efficiency.

With support from DOE (FE0009702, FE0025193, FE0029087, US-China CERC-ACTC), Washington University in St. Louis and its project partners (EPRI, Doosan Babcock, Air Liquide and West Virginia University) are developing the SPOC process with the aim to increase efficiency and reduce costs so that DOE's goals for carbon capture can be met. The SPOC approach involves staging the combustion process so that the amount of recycled flue gas can be reduced. Normally, in the absence of recycled flue gas (or another inert gas or water), oxy-combustion results in a dramatic increase in combustion temperature and radiant heat flux, as compared to combustion in air [1]. The resulting high heat flux on the boiler tubes can result in surface temperatures that exceed safe operating limits. In the SPOC process, this problem was addressed by staging the delivery of fuel while taking advantage of the optically-dense nature of pressurized coal combustion to control radiative heat flux [2-6]. This innovation allows us to maximize plant efficiency and reduce capital costs. Plant efficiencies are almost 6 percentage points better than first generation oxy-combustion [4]. Figure 1 provides a simplified process flow diagram of the SPOC process. Based on our techno-economic analysis of the process, the SPOC process meets the DOE targets set for carbon capture [2]. A recent independent analysis of the process by Hagi et al. has confirmed the dramatic efficiency improvements that can be realized by the SPOC process [7].

A critical component of the SPOC process is the Direct Contact Cooler (DCC), which is the subject of the present investigation and this final report. Because the system is under pressure, the DCC is able to capture

the latent heat of the moisture, and this additional heat can be supplied to the boiler feed water, thus increasing the efficiency of the process. In addition, as will be discussed, the high-pressure flue gas makes the system conducive to pressurized integrated pollution removal of SOx and NOx.

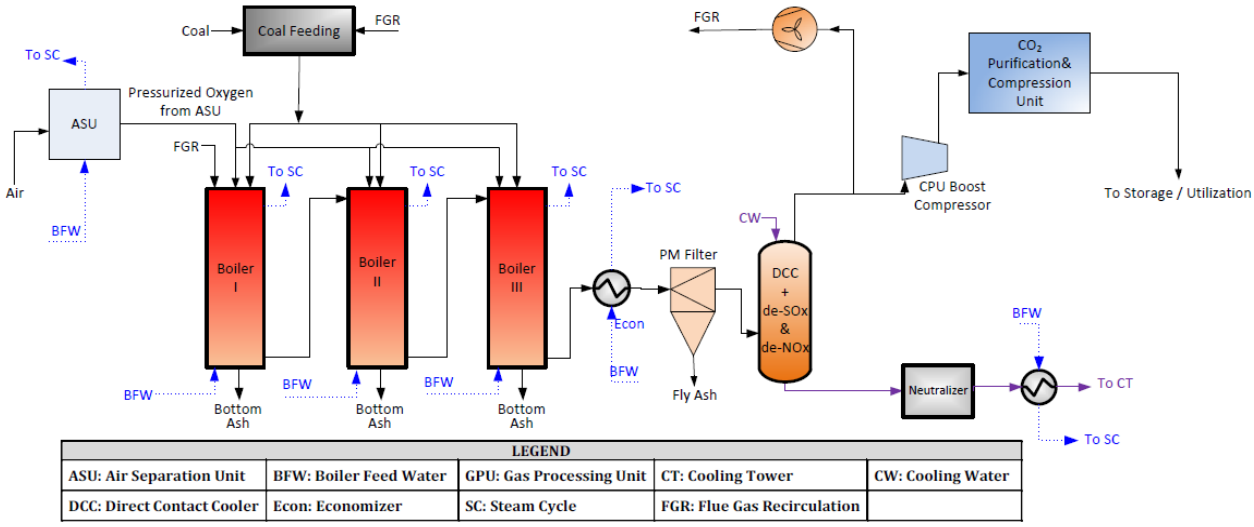

Figure 1. Process flow diagram of the SPOC process. The Direct Contact Cooler (DCC) is used to capture the latent heat of the moisture in the flue gas while simultaneously capturing SOx and NOx.

2.2 Literature Review of Sour Gas Compression for Pressurized Integrated Pollution Removal

There are currently several technologies for limiting or removing SO_x (SO_2 and SO_3^-) and NO_x (NO and NO_2) from conventional air fired power plants, *e.g.*, flue gas desulfurization, low-NO_x burners, and selective catalytic reduction. However, with pressurized oxy combustion the increased pressure allows for the use of pressurized integrated pollution removal (P-IPR) for more cost-effective and efficient scrubbing [8]. While P-IPR has been demonstrated for atmospheric oxy-combustion, this must be accomplished through compression of the flue gas, and there are intrinsic challenges in compressing a sour gas. During the cooling and pressurization of the flue gas, the pollutants may form acids – resulting in a low pH condensate, which can be damaging to equipment, such as the compressors.

The sour gas compression method has been investigated at the 30 MW_{th} Vattenfall facility [9]. Using a flue gas slipstream from a coal-fired oxy-fuel facility, White et al. [9] initially cooled the flue gas and condensed out the moisture at atmospheric pressures before an initial 15 bar(a) compression and scrubbing, followed by a 30 bar compression and scrubbing. The results indicated 80% NO_x removal after the initial 15 bar scrubbing stage, with the remainder removed in the 30 bar column. White et al. also observed the interdependence of NO_x and SO_x on the SO_x removal efficiencies, concluding that NO_x reduction prior to scrubbing may be detrimental to the SO_x scrubbing potential. However, at that time, limited information was available on the reactions occurring in the liquid phase. White et al. indicated that N_2O formation occurred in some experiments and recommended further investigation into the condensate for the identification and quantification of the sulfite and sulfate mechanism.

Wall et. al. investigated NO_x, SO_x and mercury removal from a slipstream at the Callide Oxy-Fuel plant, focusing on the effect of SO_2, residence time and temperature on conversion. Wall et al. found that SO_2 caused a minor reduction in NO oxidation but did not significantly affect overall NO_x capture. The reduction in residence time was found to reduce overall NO_x capture, whereas decreasing the temperature from 24 to 0°C provoked a large increase in capture [10].

Li et. al. [11] investigated the effect of acidic gases on the NO removal efficiency and determined that NO oxidation was the key factor. They suggested that NO_2 oxidation may be slightly impeded via gas-phase NO_2/SO_2 interactions for the formation of NO. Additionally, a comparison between a gas composition of O_2 in CO_2 and O_2 in N_2 found that the CO_2 atmosphere provides a slightly higher NO removal, attributed to carbonic acid formation, which increases the acidity of the aqueous solution and potentially facilitates NO oxidation.

In all of the above experiments, the scale was less than 20 L/min; thus, testing at larger scale is needed to confirm the results before industrial application. More importantly, the influence of flue-gas latent-heat recovery, as intended for DCC system in pressurized oxy-combustion systems like SPOC, has not been established.

2.3 Literature Review of the Relevant DCC Chemistry

A wide range of potentially relevant gas-phase, gas-to-liquid and liquid-phase reactions have been proposed to describe the chemistry in the DCC, and several reduced mechanisms have been utilized to predict SO_x and NO_x conversion efficiency in a DCC, as well as the gas and liquid outlet products. While the literature has identified the gas-phase oxidation of NO to NO_2 as a primary barrier to NO scrubbing, the effect of NO_x on SO_2 scrubbing is less well understood. Below we describe various chemical reaction mechanisms that have been proposes that are relevant to the DCC chemistry.

Elements of the scrubbing mechanism have been investigated by various authors including Raschig [12], Seel et al. [13], Yamamoto et. al [14], Oblath et al. [15] and Petrissans et al. [16]. A combined mechanism for the liquid-phase chemistry for wet flue gas scrubbing was proposed by Chang et al. [17] and is shown in Figure 2.

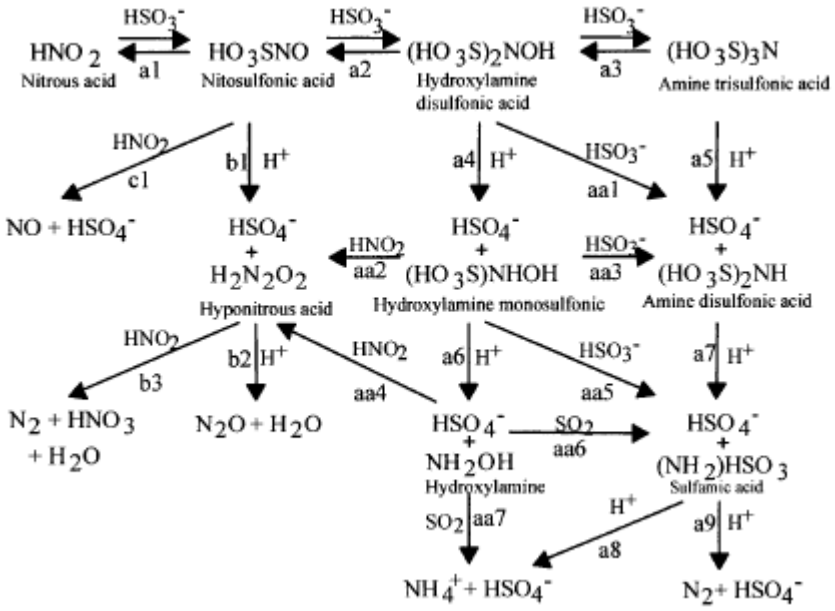

Figure 2. Reaction mechanism proposed by Chang et al. [17].

In this mechanism, the reaction pathways were distinguished in the liquid phase, resulting in the formation of 1) hydroxylamine disulfonic acid (HADS) and other complexes, and/or 2) sulfuric acid and/or nitrogen

compounds. Petrissans et al. [16] noted that the primary pathways for these reactions are dependent on pH, temperature and the stoichiometric ratio of bisulfate and nitrate ions.

While information on the liquid-phase chemistry is limited, a number of studies to model scrubbing have been conducted recently. Normann et al. identified up to 33 individual gas and liquid reactions that may play a role in the gas, gas/liquid or liquid chemistry [18]. Normann et al. identified that a key role in the scrubbing chemistry is the complex interactions between HNO_2 and HSO_3^-, which are capable of enhancing the oxidation rate to produce HNO_3 and H_2SO_4. They achieved this by modeling the formation of HNO_3 and H_2SO_4 through several unstable intermediaries, including $NOSO_3^-$ and HNO, resulting in approximately eight liquid-phase reactions. Importantly, Normann et al. concluded that further investigation into the interaction between the liquid ions, especially at pH greater than 0, should be a priority.

Figure 3 shows a simplification of the overall mechanism for NO and SO_2 conversion and indicates the key gas-gas, gas-liquid and liquid-liquid reactions.

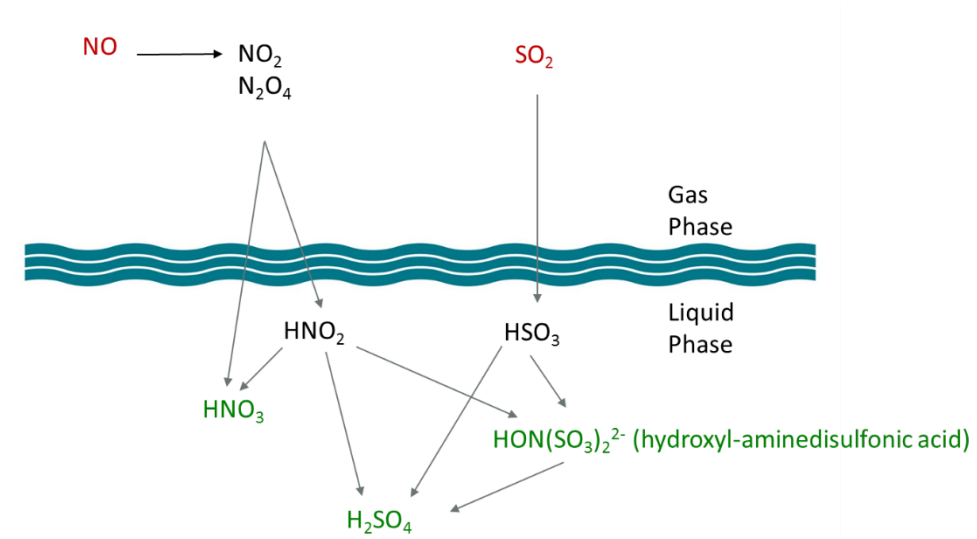

Figure 3. A simplified mechanism of NOx and SOx removal [15].

Following a sensitivity analysis of the primary reactions, Ajdari et al. [19] proposed a reduced mechanism of between 7 and 12 reactions based on the operational pH of the system, and it was concluded that the gas-

phase reactions are limited by NO oxidation, whereas the liquid-phase interactions are predominantly pH controlled. The liquid-phase mechanism was streamlined based on Equations 1 and 2,

$$HNO_2 + HSO_3^- \rightarrow HSO_4^- + \frac{1}{2}N_2O + \frac{1}{2}H_2O \quad (1)$$

$$HNO_2 + 2HSO_3^- \rightarrow HON(SO_3)_2^{2-} + H_2O \quad (2)$$

both of which are combinations of formation and consumption reactions for several unstable intermediaries to form a stable product. However, Ajdari also recommended further investigation of liquid chemistry.

Ajdari's mechanism formed the basis for the modeling of a full-scale DCC scrubbing column by Tumsa et al. [8]. Tumsa modeled a column with a 120 kg/s gas flow in a 5.2 m dimeter, 14 m high packed-bed column. The model discretized the column into 12 stages with the individual liquid- and gas-phase concentrations calculated. The formation of the major liquid concentrations showed that H_2SO_4 formation occurs at the back end of the column while HSO_3^- forms rapidly at the inlet. Tumsa varied the L:G ratio, recycle, pH and N:S ratio and determined that the process was strongly pressure dependent and the gas purity requirements dictated the recycle ratio within the system – as a reduced pH significantly affects the gas outlet purity. Tumsa concluded that an operating pressure of 30 bar, temperature of 40°C and a non-recycled L:G ratio of 1.5 – 3 would result in almost complete removal of SO_x and NO_x. However, once again this modeling effort is not based on using P-IPR for flue-gas latent-heat recovery as well. When used in this way, which improves cycle efficiency, the operating conditions are dictated by the need to efficiently recover the latent heat in the flue gas moisture. Thus, to allow for application to a DCC in pressurized oxy-combustion, further studies are necessary.

3. Project Objectives and Scope

The overall objective of this project was to develop an enabling technology for simultaneous recovery of latent heat and removal of SOx and NOx from flue gas during pressurized oxy-coal combustion, so as to

maximize efficiency, eliminate conventional FGD and de-NOx processes and minimize the cost of electricity. The R&D effort included performance tests at a 100 kW scale to validate the process and obtain key engineering data for scale-up. A collateral objective was to study the gas and liquid phase kinetics, and the development of a systematic chemical mechanism validated by experimental data. With this information, full-scale process modeling of the DCC was performed to evaluate equipment size and performance.

The scope of work consisted of experiments at two scales, bench-scale and 100 kW scale. The team conducted bench-scale experiments in a continuously-stirred reactor to confirm key liquid-phase reaction rates at various temperatures to validate the proposed chemical mechanism (Section 4). A prototype 100 kW DCC column was constructed and installed in the pressurized oxy-combustion facility at Washington University in St. Louis. The performance of this prototype was evaluated using simulated flue gas, and the SOx and NOx capture efficiency was determined under a wide range of operating conditions (Section 5). In parallel, an ASPEN process model of the column was created and updated based upon experimental data for future scaled-up engineering development studies. Finally, the model was used to simulate a full scale DCC and evaluate the optimum configuration for the DCC (Section 6).

4. Lab-Scale CSTR Experiments to Understand Liquid-phase Chemistry

The objectives of this study were to investigate the two primary Equations 1 and 2 at conditions relevant for pressurized flue gas scrubbing, emphasizing the effect of lower pH and elevated temperatures at short time scales.

4.1 Materials and Methodology

The reactions were studied in the aqueous phase using a 100 mL stirred borosilicate reactor, with the temperature regulated using a water bath. Aqueous solutions were formed for HNO_2, HNO_3 and HSO_3^- using $NaHSO_3$ (Reagent Grade), $NaNO_2$ (A.C.S Reagent Grade) or $NaNO_3$(A.C.S. Reagent Grade) and

deionized water. The solutions were combined with phosphoric acid, creating standard solutions with known pH. HNO_3^- is expected to be generated in scrubbing systems through NO_2 dissolution, however for the liquid-phase chemistry it is considered unreactive under acidic or mildly acidic conditions [20] and was used in the experiments as a normalization standard. As the experiments required several stages of dilution, the variation in HNO_3^- concentration provide a correction factor for the HNO_2, HSO_3^- and HSO_4^- concentrations.

The solutions were combined to generate initial vessel concentrations of 3×10^{-3} M HNO_2 and HSO_3^- concentrations in a 50 mL vessel. Once mixed, samples were taken as frequently as possible over a 5-minute period and stored for analysis.

The storage methodology was adapted from Petrissans et al. [16] and conducted utilizing a combination of $1x10^{-3}$ M (A.C.S Reagent Grade) D-mannitol solution at a pH of 12. Sodium hydroxide and phosphoric acid were chosen to control the pH, as they do not interfere with the liquid chemistry. The high pH blocks any sulfite and nitrite interactions, while the D-Mannitol prevents sulfite oxidation, providing a stable solution for sample storage.

The analysis of the sample was conducted using ion chromatography (Dionex ICS-1600), with an IonPac AG22 column and an ASRS 300 Suppressor capable of quantifying HNO_2, HNO_3^-, HSO_3^- and HSO_4^- concentrations. This column was unable to detect the presence of HADS, however the accurate determination of the initial ion concentration coupled with a mass balance, provides the formation rate of the individual reactions with the methodology discussed below.

4.2 Results and Discussion

a. The Nitrogen System

Prior to experiments with sulfur, experiments with nitrogen only were conducted to determine the potential for NO(*g*) formation from the liquid-phase chemistry as well as the nitrogen dissolution in the liquid phase. Equation 3 below, which results in the generation of unwanted NO(*g*) [21], was investigated:

$$3HNO_2 \rightarrow HNO_3^- + 2NO + H_2O \quad (3)$$

The experiments were conducted in a 15 bar(a) pressure vessel with a 50 mL mixture of either NO/O_2 or NO_2 gases with 250 mL of deionized water. The liquid concentrations were investigated via ion chromatography to establish the formation and change in HNO_2 and HNO_3^-.

From Figure 4, the liquid phase shows a 1:1 ratio between HNO_2:HNO_3^- which does not change at residence times up to 60 minutes. The 1:1 ratio suggests that the gas dissolution can be described by Equation 4.

$$2NO_2 + H_2O \rightarrow HNO_3^- + HNO_2 \quad (4)$$

Continually, the 1:1 ratio along with the stable ion concentration after 60 minutes show that Equation 3 does not occur to an observable extent. This was also confirmed via the analysis of the gas phase in Figure 4 (b) with no NO observable in the gas-phase analysis. These results confirmed that Equation 3 can be excluded from the reduced kinetic model of the system.

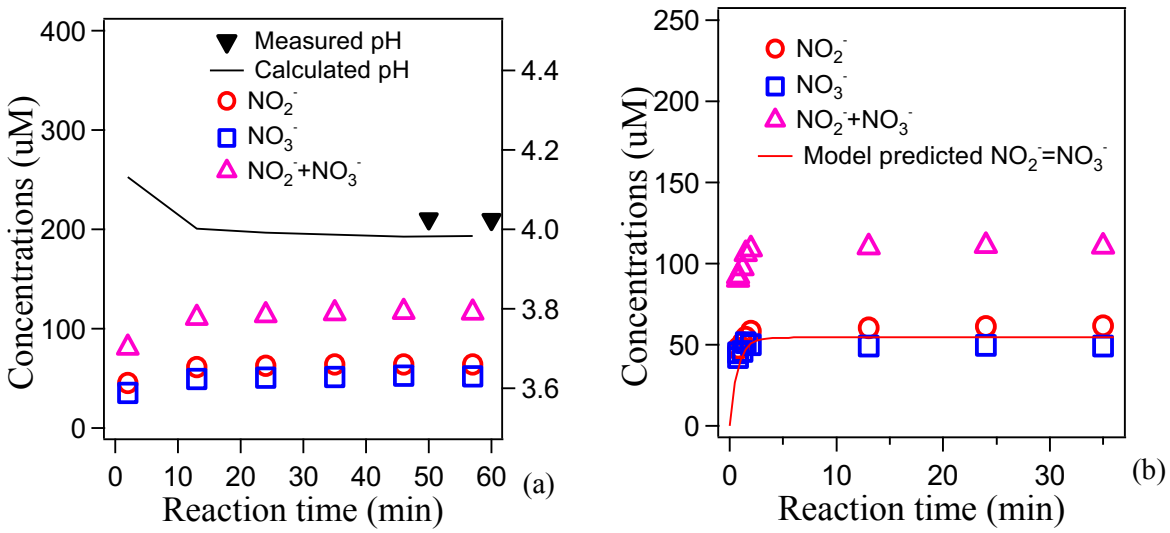

Figure 4. HNO_2^- and HNO_3^- liquid ion formation from (a) 900 ppm NO/ 3% O_2 and (b) 900 ppm NO_2 gas mixtures.

b. The Nitrogen and Sulfur system

The consumption and formation rates are determined via the concentration of the HNO_2, HSO_3^- and HSO_4^- in a reactor, with a characteristic curve shown in Figure 5. The graph displays the reduction in HNO_2 and HSO_3^- concentrations and the formation of HSO_4^-. However, the observed ratio of HSO_3^- consumption with HSO_4^- formation is not 1:1, as defined in Equation 1. Quantifying the difference in consumption of HSO_3^- and the formation of HSO_4^-, leads to an incomplete sulfur balance. Using a similar method for nitrogen, based off of the stoichiometry of Equation 1, i.e., $[HSO_4^-] = ½ [N_2O]$, an incomplete mass balance is also observed. Previous papers associated this imbalance with an unknown complex or combination of complexes [16], with the formation of the HADS complex (Equation 1) being indirectly proven via the 'missing' N:S ratio being approximately 1:2, which is the molar ratio of HADS. Petrissans et al. showed this ratio was 1.73 at pH 4 and 1.94 at pH 5. In comparison, our experimentally observed ratio at pH 3 was approximately 2.1 – 2.2 and is close to the HADS ratio. Thus, for the purposes of this work, the incomplete mass balances are attributed to the formation of HADS. This is consistent with the assumption of the two major liquid chemistry reactions given by Equations 1 and 2.

Several papers discuss the potential for the hydrolysis of HADS to further form the complex HAMS (hydroxylamine monosulfonic acid – $HONHSO_3^-$). However, HAMS accounts for a small percentage of the N-S complexes formed [19]. Investigations into HADS by Ajdari et al. [20] indicated that the formation of HAMS accounts for less than 10% of the total HADS formation after a 10-minute period. The formation is strongly pH dependent, and was considered to be insignificant at a pH above 2 [20]. Thus, the formation of HMS was neglected in this work.

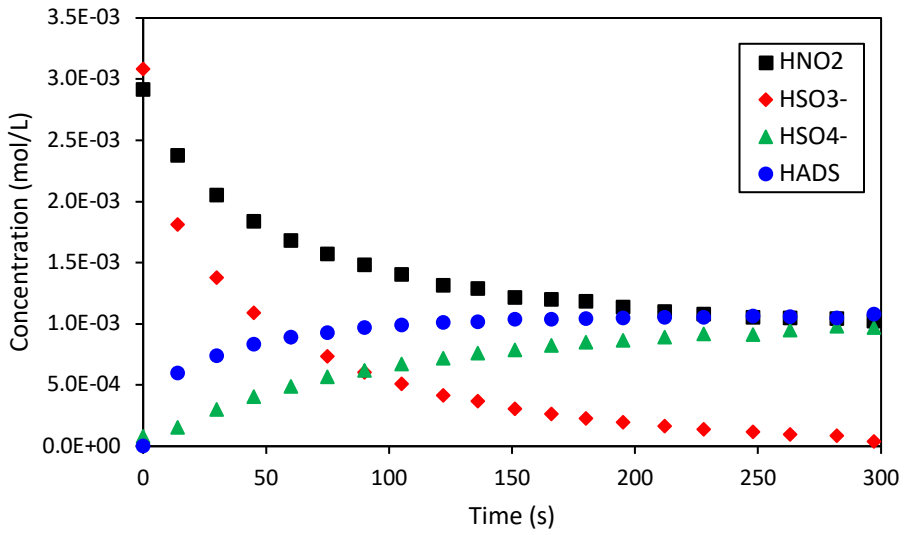

Figure 5. Liquid concentrations of HNO_2 and HSO_3^-, HSO_4^- and HADS at pH = 3 and 22°C.

c. The effect of pH

The pH was varied between 2.5 and 4 to investigate the change in rates for Equations 1 and 2. The concentrations of HNO_2 and HSO_3^-, HSO_4^- and H^+ were measured, and the species used to identify Equations 1 and 2 were HSO_4^- and HADS (based on calculation), respectively.

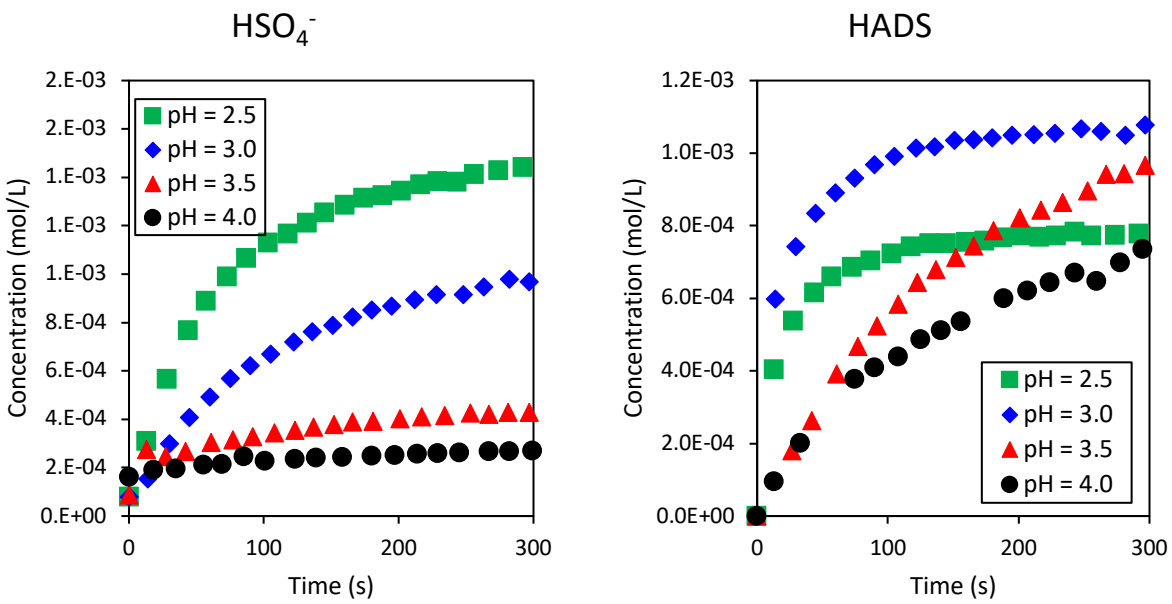

Figure 6. The effect of pH on HSO_4^- and HADS formation rate at 22 °C.

Figure 6 shows that a decrease in pH results in an increase in HSO_4^- formation rate. This indicates that Equation 1 is more prevalent at lower pH, which is corroborated with results from Pires et al. [22], where they found that the rate of formation of N_2O is a maximum at pH of 0. This was also observed experimentally by Petrissans et. al [16], where they found a pressure increase (correlated with N_2O formation, i.e., gas formation) at lower pH.

The formation of HADS shows a more complex dependence on pH, with HADS concentration increasing as pH goes from 4 to 3 and then reducing at 2.5. From the literature, the HADS concentration is expected to decrease at lower pH, however, the initial increase in rate from pH 4 to pH 3 is unexpected. We attribute this to a combination of consumption of H^+ within the system along with the shorter timescales of our experiments. In the previous literature, the solutions were buffered to provide a single pH; however, our batch system allows the investigation of H^+ as a reactant. While a significant change in H^+ was only observed for pH = 4, the initial H^+ concentration was $1x10^{-4}$ M and reduced to $6x10^{-5}$ M before the reaction

ceased, suggesting Equation 2 ceased due to a lack of reactants. When the pH decreases, the H^+ is in excess by orders of magnitude, and is never consumed fully. With respect to timescales, a higher pH results in slower reaction rates for the formation of HADS, with previous studies suggesting complete reaction after 20 to 30 minutes for pH = 4. Due to the shorter timescales in our experiments, the reaction was not complete and therefore the HADS concentration did not reached its maximum, and consequently the HSO_3^- concentrations was comparably high.

d. The effect of temperature

In Figure 7, the increased temperatures results in an increased reaction rate for both HSO_4^- and HADS. While the HADS formation has only a minor increase in rate, the HSO_4^- rate rapidly increases - however the maximum concentration appears to be reduced. The reduction in HSO_4^- concentration is balanced by the presence of a non-reacting concentration of HSO_3^- in the system. In the 80°C experiment, approximately 5% of the total sulfur in the vessel is HSO_3^-. The presence of HSO_3^- in the liquid is interesting in regards to the operation of high temperature gas scrubbing. As SO_2 scrubbing occurs via the equilibrium gas reaction $SO_2 \leftrightarrow HSO_3^-$ and relies on liquid-phase chemistry to remove the HSO_3^-, the non-consumption of HSO_3^- means the effective SO_2 adsorption rate may decrease.

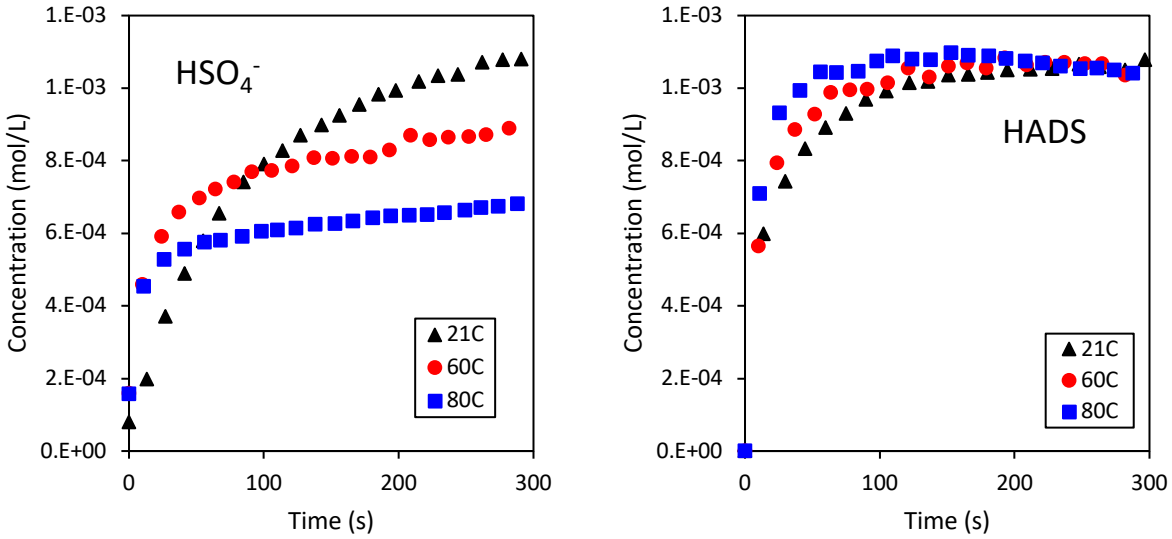

Figure 7. The effect of temperature on HSO_4^- and HADS formation.

An interesting result for the increase in temperature is that the HADS concentration decreases over extended periods of time. At elevated temperatures and longer residence times, the concentrations of HNO_2, HSO_3^- and HSO_4^- no longer appear stable.

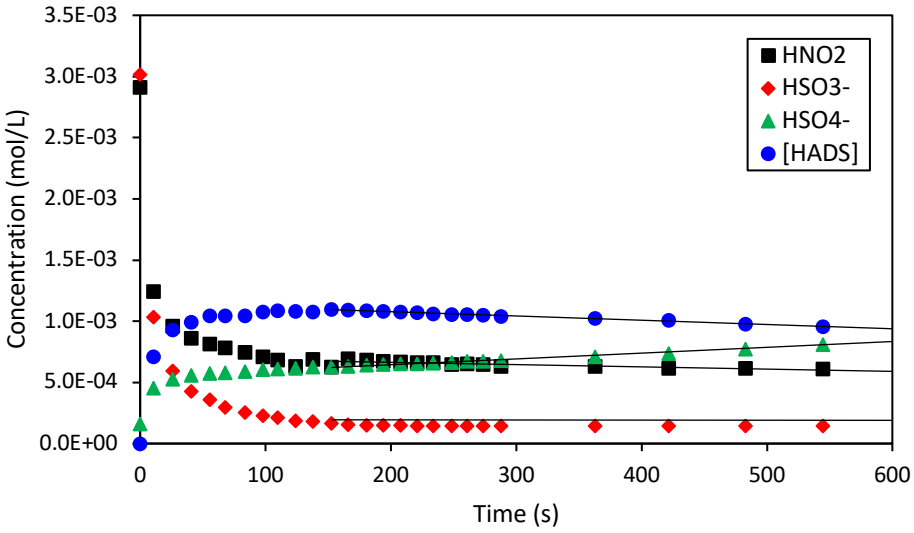

Figure 8. Species concentration at elevated temperatures at pH = 3 and a temperature = 80°C.

Figure 8 shows HNO_2 continues to decrease without any change to the HSO_3^- concentration, which is not accounted for in the current reaction mechanism. Correlating the HADS concentration to the HSO_3^-, HNO_2 and the HSO_4^-, a further reaction is taking place resulting in the formation of HSO_4^- in conjunction with the consumption of HNO_2. A molar balance taken of the consumption and formation rates of HNO_2 and HSO_4^- show a 1:2 ratio of nitrogen to sulfur and, based on the previously established mechanisms, the reaction chemistry can be hypothesized. From the Chang et al. [17] reaction mechanism in Figure 2, two potential reaction pathways for the consumption of HNO_2 and the formation of HSO_4^- are present, and are denoted in Figure 2 as either a4 or b1. The b1 pathway is based on a reverse equilibrium reaction for HADS to revert to nitrosulfonic acid and be consumed via the formation of $H_2N_2O_2$, and finally N_2O (Equations 5-7), with the generated HSO_3^- reacting with HNO_2.

$$HON(SO_3)_2^{2-} \rightarrow HSO_3^- + HO_3SNO \quad (5)$$

$$HO_3SNO + H^+ \rightarrow HSO_4^- + H_2N_2O_2 \quad (6)$$

$$H_2N_2O_2 + H^+ \rightarrow N_2O + H_2O \quad (7)$$

The b1 pathway results in the formation hydroxylamine monosulfonic acid, Equation 8, followed by its interaction with HNO_2 for the formation of $H_2N_2O_2$ and finally N_2O (Equations 9 and 10). This pathway has been outlined in Ajdari et al. [19], however their sensitivity analysis disregarded it as relevant. In comparison, the b1 pathway is unclear, as different literature regard it as either reversible or irreversible. However, both reaction mechanisms result in the same overall reaction equation, Equation 9:

$$HON(SO_3)_2^{2-} + H^+ \rightarrow HSO_4^- + (HO_3S)NHOH \quad (8)$$

$$(HO_3S)NHOH + HNO_2 \rightarrow HSO_4^- + H_2N_2O_2 \quad (9)$$

$$H_2N_2O_2 + H^+ \rightarrow N_2O + H_2O \quad (10)$$

$$HON(SO_3)_2^{2-} + HNO_2 \rightarrow N_2O + H_2O \quad (11)$$

While Equation 9 results in the same products as Equation 1, the influence of temperature on the previously stable complex (HADS) means Equation 6 requires further investigation to determine the rate limiting step and the assumptions needed for modeling. Our results indicate that at 80°C the rate of Equation 11 appears to be 4.74 x 10^{-7} $mol.L^{-1}.s^{-1}$

e. Comparisons with existing rate formation models

A determination of the kinetic rate model for HADS has been previously established in Oblath et al. [15] over a temperature range of 15 – 30°C, a pH of 4.5 – 6.5 and an ionic strength of 1.2 mol/L:

$$\frac{d[HADS]}{dt} = k_0[H^+]^2[NO_2^-] + k_I[H^+][NO_2^-][HSO_3^-] + k_{II}[NO_2^-][HSO_3^-]^2 \quad (12)$$

where $k_0 = 8x10^5$; $k_I = 3.7x10^{12}e^{-6100/T}$; $k_{II} = 9x10^{-4}e^{2.1(\mu)^{1/2}}$ (T in Kelvin, μ is ionic strength in mol/L). Petrissans et. al [16] determined that the first and third terms are not relevant due to the pH range and low bisulfite concentration respectively, and corroborated a K_1 value of 3990 $L.mol^{-2}s^{-1}$, similar to Oblath. In both cases the experiments were conducted at high pH to reduce interference from Equation 1.

In Figure 9, the Petrissans and Oblath models are compared to the HADS formation observed in the experiments. The Petrissans model shows a good fit with a minor underestimation of HADS formation whereas the Oblath model shows a large overestimation in HADS concentration, attributed to the first term, $k_0[H^+]^2[NO_2^-]$. This term, neglected by Petrissans, is not a function of HSO_3^- concentration, since it is in excess, resulting in a reaction rate term which never reaches zero. While not shown, this term becomes dominant at lower H^+ concentrations, further affecting the predicted HADS concentration.

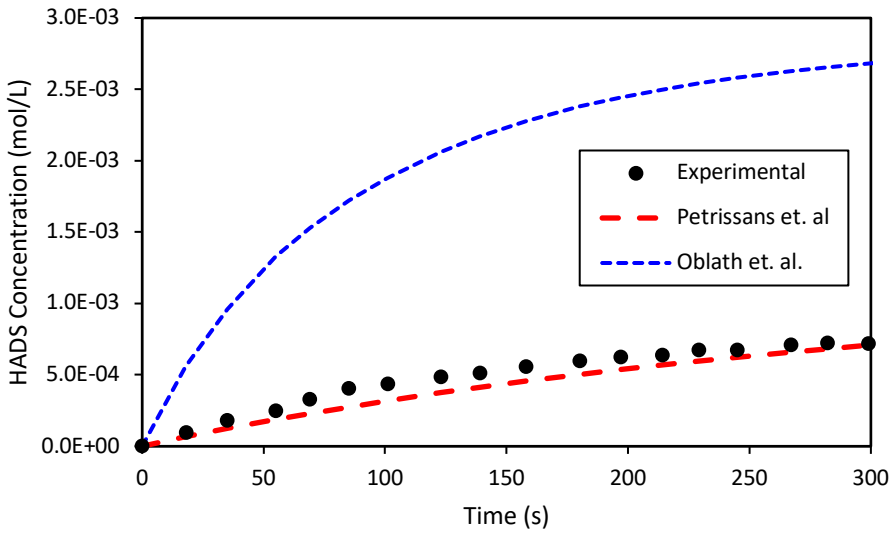

Figure 9. A comparison between experimental data and HADS prediction at a pH of 4

The formation of the HSO_4^- has been described by several sequential reactions. From the reaction mechanism observed in Figure 2 and discussed in Ajdari et al. [19], the formation of HSO_4^- in Equation 1 is based on Equations 5-7. However, Ajdari determined that the rate limiting step was the formation of the initial complex, NSS, shown in Equation 13:

$$HNO_2 + HSO_3^- \rightarrow ONSO_3^- + H_2O. \quad (13)$$

The formation of the intermediary has been defined from Oblath et. al [23] based on the partial conversion during the formation of HADS. Taken from Normann et al. [18], the form of the reaction rate equation for the formation of HSO_4^- is:

$$\frac{d[HSO_4^-]}{dt} = k_1 \times [NO_2^-][HSO_3^-] \quad (14)$$

with $k_1 = 2.4 \pm 0.5$.

As the experiments which form HSO_4^- also result in the formation of HADS, the prediction of HSO_4^- was run in parallel with the HADS formation and compared to the experimental data at a pH of 3. The results,

shown in Figure 10, show reasonable agreement with the formation of HADS in the system and an initial overestimation of the HSO_4^- formation, with corresponding overestimation of consumption of reactants HNO_2 and HSO_3^-. The prediction of HSO_4^- is less accurate, with an overprediction (~175%) at early times and a slight underprediction at steady-state (~20% error).

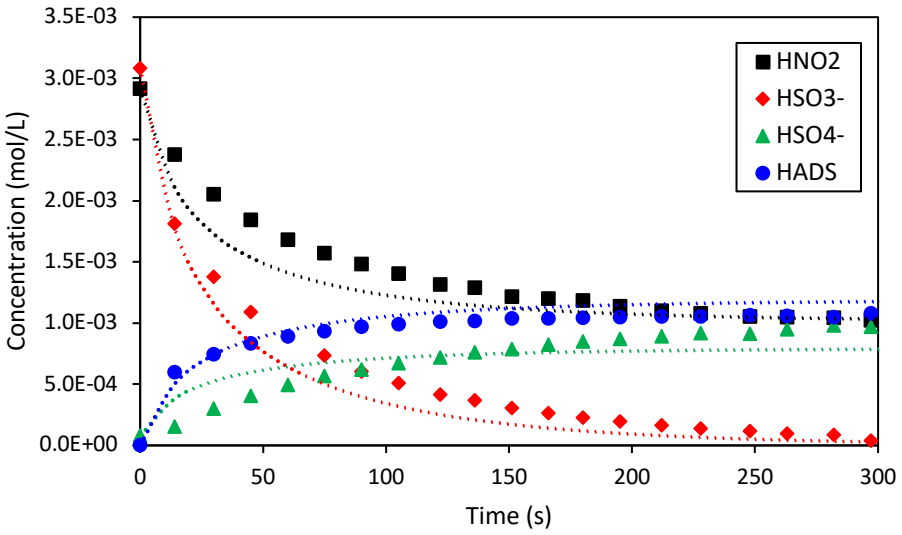

Figure 10. Comparison between HSO4- prediction and experimental data at pH = 3.

The above results indicate that the reaction rate constants given in the literature provide an accurate prediction for a pH range between 3 and 4. However, at lower pH, new rate constants are needed. Low pH systems could not be accurately represented using both the full Oblath Equation 10 and the reduced Petrissans equation (second term in Equation 12). At a pH of 2.5 the experimentally determined HADS formation rate was 3.1×10^{-5} $mol.L^{-1}s^{-1}$. In comparison, the values from the Oblath and Petrissans models were 2.3×10^{-2} $mol.L^{-1}s^{-1}$ and 1.4×10^{-4} $mol.L^{-1}s^{-1}$ respectively.

4.3 Conclusions

The presented work shows an updated understanding of the liquid chemistry relevant for a pressurized flue gas scrubbing system. The two reactions rates, $HNO_2 + HSO_3^- \rightarrow HSO_4^- + \frac{1}{2}N_2O + \frac{1}{2}H_2O$ and $HNO_2 + 2HSO_3^- \rightarrow HON(SO_3)_2^{2-} + H_2O$ have been calculated via the measured HSO_4^- concentration increase and an incomplete mass differential between HSO_3^- and HSO_4^-. The effects of temperature (21 – 80°C) and pH (2.5 to 4) were observed. Increasing temperature results in an increased reaction rate for HSO_4^-, but a reduced equilibrium concentration. Comparatively, the initial HADS concentration shows relatively little change with temperature. However at higher temperatures HADS becomes unstable, consistent with the reaction: $HON(SO_3)_2^{2-} + HNO_2 \rightarrow N_2O + H_2O$. This indicates a temperature dependent reaction, which is currently not accounted for in flue gas scrubbing models.

5. DCC Scale Experiments

5.1 Materials and Methodology

Experiments were conducted in a direct contact column (DCC) which was constructed for this project and is shown in Figures 11 and 12. The column was designed by Process Engineering Associates, LLC with the vessel fabrication, piping and instrument assembly performed by Progressive Recovery, Inc. Synthetic flue gas was created and passed through the DCC under a variety of temperatures, pressures, flowrates and compositions to parametrically investigate the NO_x and SO_2 scrubbing efficiency. The flue gas is fed at the bottom of the column while water is fed and distributed at the top. A packed bed with an 8-inch diameter and a 7-foot 6-inch height, consisting of 316 stainless steel saddle rings (Interlox), is used to create high surface areas and high gas and liquid contact areas, which allows the gaseous pollutants to be adsorbed into the liquid phase. The water, which has been acidified, is collected in the sump tank before leaving the column. The purified gas leaves the top of the column and is analyzed for SO_2 and NO_x concentration.

The DCC system was sized based on outlet conditions for a 100 kW_{th} pressurized oxy-fuel flue gas combustor. The base case for the simulated dry flue gas composition is shown in Table 1 with 800 SLPM gas flowrate, a gas inlet temperature of 22°C with an L:G ratio of 0.95 ($kg_{(l)}$:$kg_{(g)}$). As pollutant concentrations are dependent on coal composition and burner design, 500 ppm of both NO and SO_2 were chosen, based on approximate pollutant concentrations typically encountered using low sulfur coals in oxy-combustor systems [24].

Table 1. Base-Case Gas Inlet Composition

Species	Volume
O_2	3 %
CO_2	95 %
N_2	2 %
SO_2	0.05 %
NO	0.05 %

Figure 11. DCC scrubbing column installed at the pressurized oxy-combustion research facility at Washington University in St. Louis.

The synthetic pressurized flue gas was generated via injection of SO_2 (3% SO_2/N_2 mix) and NO (10% NO/N_2 mix) (Praxair) into the CO_2 line. The gas mixture was subsequently heated with an electric in-line heater. Oxygen was added to the heated gas at the reactor inlet, to avoid oxidation of NO to NO_2 in the gas delivery system, such that the initial concentration of NO at the reactor inlet could be determined. The gas composition at the reactor inlet and outlet was measured using a PG-250 HORIBA gas analyzer, which measured total NO_x ($NO + NO_2$), SO_2 and O_2 concentrations.

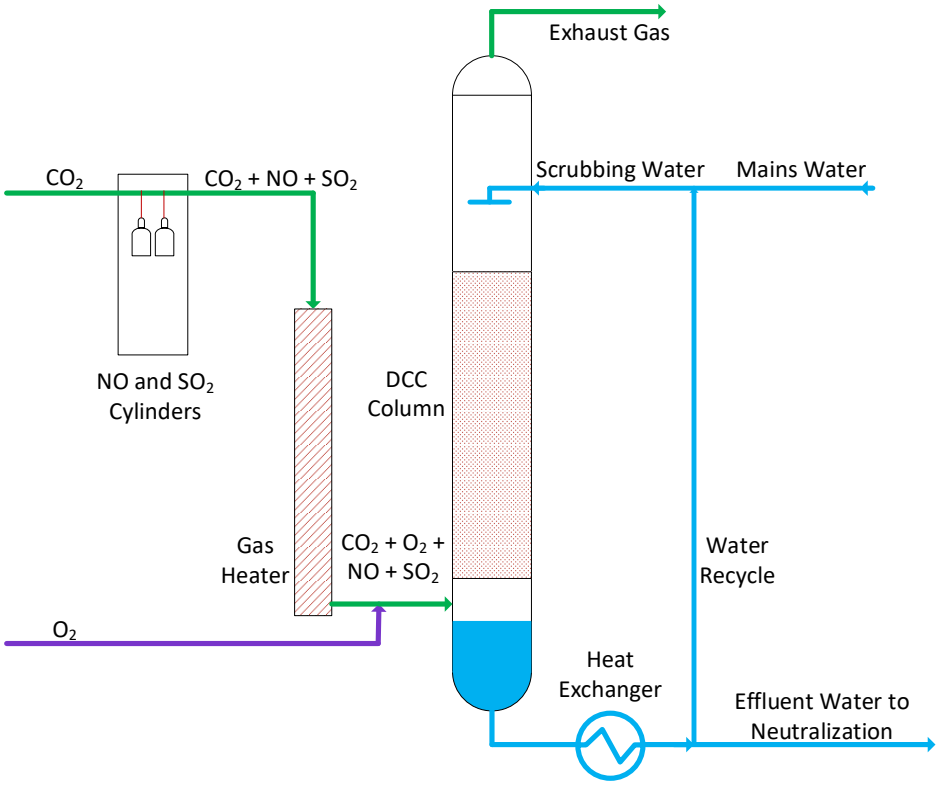

Figure 12. DCC Column Schematic.

In all experiments, fresh city water was supplied to the DCC with a pH ≈ 9. While the system is capable of water recycle to provide additional pH control, as shown in Figure 12, it was determined that this was not necessary to achieve good results and the system was operated in a once-through fashion. The liquid discharged from the sump typically had a pH ≈ 2.4, which varied only slightly within the range of L:G ratio and inlet pollutant concentrations considered in this study.

A rate-based reactive absorption column was modeled using the RadFrac unit in Aspen plus V9 with the dimensions and internals of the DCC column. ELECNRTL was used as a property method because of its compatibility with the system in both liquid and gas phase. The reactions used for the simulation are described in Table 2, with the equilibrium reactions handled directly in ASPEN. For the kinetic reactions, Reactions 1 and 7 were supplied through a kinetic sub-routine written separately and kinetic parameters for Reaction 5 and 6 were provided in form of power-law expression in ASPEN.

Table 2. Reduced DCC Scrubbing Mechanism

Reaction Number	Reaction	Type	Reference
1	$2NO + O_2 \rightarrow 2NO_2$	Kinetic	[25]
2	$2NO_2 \rightarrow N_2O_4$	Equilibrium	
3	$2NO_2(N_2O_4) + 2H_2O \rightarrow HNO_2 + NO_3^- + H_3O^+$	Equilibrium	
4	$SO_2 + 2H_2O \leftrightarrow H_3O^+ + HSO_3^-$	Equilibrium	
5	$HNO_2 + HSO_3^- \rightarrow 1/2N_2O + HSO_4^- + 1/2H_2O$	Kinetic	Our data
6	$HNO_2 + 2HSO_3^- \rightarrow HADS + H_2O$	Kinetic	Our data, [15, 23]
7	$NO_2 + SO_2 \rightarrow NO + SO_3$	Kinetic	[26]
8	$SO_3 + H_2O \leftrightarrow HSO_4^-$	Equilibrium	

5.2 Results and Discussion

a. Investigation of NO oxidation within the column

The rate-limiting step in NO_x scrubbing has been previously tested and discussed in literature and has been attributed to the oxidation of NO to NO_2 [19]. This conclusion is corroborated by the results in Figure 13, which shows the measured instantaneous and steady-state outlet concentration of NO_x as a function of the outlet oxygen concentration. The experiment was conducted at 13.5 bar(a) and the oxygen concentration in the synthetic flue gas was varied up to approx. 4 %vol., which is consistent with typical oxygen levels in pulverized coal boiler flue gas. Results indicate that NO conversion is very sensitive to oxygen partial pressure, in the range of 0 to 0.1 bar, but approaches a constant value at higher oxygen levels. In this experiment, the minimum outlet NO concentration attained was 55 ppm, which corresponds to a capture efficiency of 92%.

Based on the oxygen concentration, pressure and vessel residence time the NO oxidation rate was calculated to predict the formation of NO_2 within the vessel according to Reaction 1 in Table 2. Assuming the instantaneous NO_2 adsorption into the liquid phase, a comparison can be made between the NO oxidation model and the measured NO_x outlet concentrations. For this calculation, the gas-phase residence time of

120 seconds was determined by considering the packing volume and tortuosity and the pre- and post-packing volumes. Figure 13 shows the NO outlet concentration at steady state is in line with the instantaneous NO_x outlet concentration, showing that instantaneous NO_x concentrations can be used for the analysis of low oxygen partial pressure conditions.

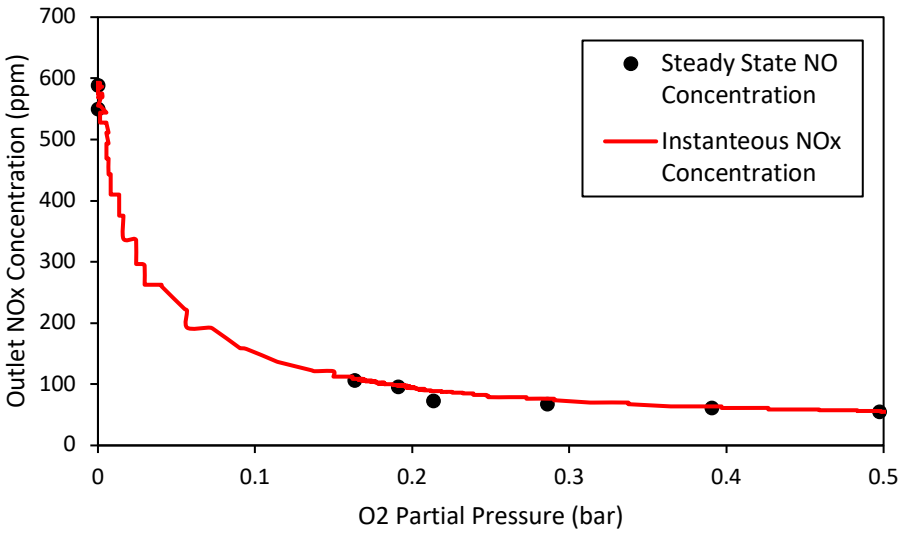

Figure 13. NO_x outlet concentrations in a 13.5 bar, 22°C DCC system.

Table 3. Operation Conditions Corresponding to Figure 13

Parameters	
Pressure	13.5 bar(a)
Temperature	24 °C
Gas Flowrate	777 SLPM
L:G Ratio	0.94 $kg_{(l)}$:$kg_{(g)}$
Residence Time	120 seconds
NO Inlet Concentration	566 ppm
SO_2 Inlet Concentration	421ppm

b. The influence of oxygen partial pressure on NO_x and SO_2 capture

Since NO oxidation was identified as the rate-limiting step, the effects of total pressure, oxygen partial pressure, and residence time on NO_x and SO_2 scrubbing were experimentally investigated in more detail to determine optimal operating conditions. The operating pressure was varied while holding the mass flow

rate of gas constant. Figure 14 shows the change in NO_x capture as a function of O_2 partial pressure at four different pressures. Each curve in Figure 14 was obtained by increasing the oxygen concentration from zero to the maximum, and then decreasing back to zero to capture any hysteresis effects. Each data point was collected with a 1 second resolution. Figure 14 shows that the reduction in pressure from 15 bar (130 seconds residence time) to 11 bar (95 seconds) yields a maximum decrease in NO_x scrubbing efficiency of approximately 10% when the O_2 partial pressure is less than 0.25 bar. The difference within this range is reduced at higher O_2 partial pressures, with partial pressures greater than 0.25 bar showing NO_x capture approaching 90% within these residence times. However, when pressure was further reduced to 9 bar (78 seconds residence time), the NO_x conversion was more severely affected. From Figure 14, the results indicate the minimal residence time for NO_x scrubbing in this system would be approximately 95 seconds.

Throughout the experiments described above, a high SO_2 removal efficiency in the range of 93–100 % was consistently observed. Removal efficiency of less than 100% was only observed is cases when the oxygen concentration was effectively zero. The removal of SO_2 is discussed in more detail in the following sections.

A range of gas-phase NO oxidation models have been developed in the literature and the variation in kinetic constants in these models can lead to significant variability in predictions for NO concentration [24, 25, 27, 28]. The NO oxidation model utilized in this work is from Tsukahara et al. [25] with the form:

$$\frac{d(NO)}{dt} = 2k[NO]^2[O_2] \quad (13)$$

Where $k = 1.2 \times 10^3 \times e^{530/T}$, with T in Kelvin. There is no consensus for a detailed mechanism for NO oxidation, with 3 systems proposed. The first is a termolecular reaction, the second is a two-step $(NO)_2$ intermediate system and the last is a two-step (NO_3) intermediate [27]. Recent literature typically uses the two-step $(NO)_2$ mechanism to describe NO oxidation [25].

Based on Equation 13 and the observations in Figure 14, the kinetic constant (k) was recalculated for the experimental results. Shown for 15 bar (130 seconds) and 9 bar (78 seconds) the kinetic constant was determined to be $k = 2.1 \times 10^3 \times e^{530/T}$. The constant was calculated by a sum of least squares method with

the best fit kinetic constant (k) found for every NO conversion value observed in Figure 14. This kinetic constants it is approximately 75% higher than Tsukahara et. al. [25] and above the upper range discussed in Greig and Hall [29, 30] and Morrison et. al. [31]. The new kinetic constant shows an overestimation of capture of approximately 5% at 9 bar. The 15 bar results are in good agreement, underestimating O_2 partial pressures by less than 0.04 bar. The difference in k can be attributed to a longer residence time than anticipated, the limitations of the experimental sensors (HORIBA) used, or the presence of a secondary gas phase reaction.

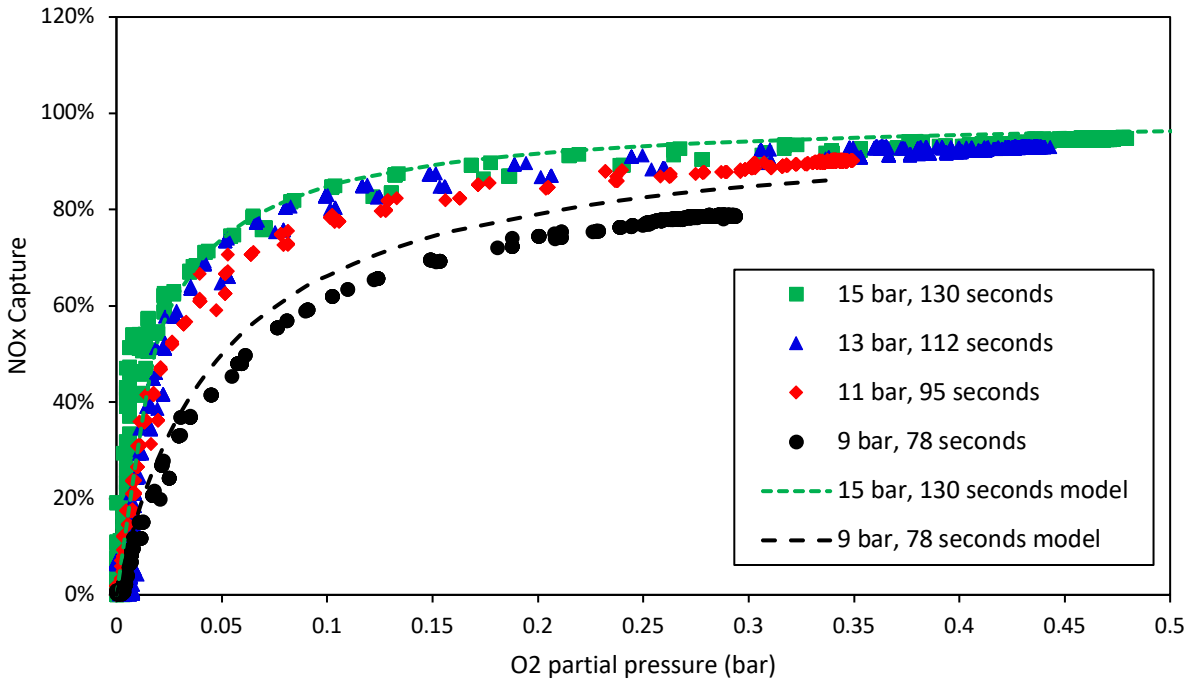

Figure 14. The effect of residence time and oxygen partial pressure on NOx capture.

Table 4. Operation Conditions Corresponding to Figure 14

Parameters	
Pressure	9 -15 bar(a)
Temperature	23 °C
Oxygen Concentration	0 – 3.1 %

Gas Flowrate	801 SLPM
L:G Ratio	0.97 $kg_{(l)}$:$kg_{(g)}$
Residence Time	130 – 78 seconds
NO Inlet Concentration	530 ppm
SO_2 Inlet Concentration	530ppm

c. The influence of N:S ratio on conversion

While the gas-phase and gas-to-liquid-phase chemistry is relatively well understood, the literature suggests that the presence of NO_x within the gas phase results in an increase in uptake of SO_2. An investigation of the N:S ratio was conducted to observe the influence of NO on SO_2 conversion, with the base conditions shown in Table 5. A 530 ppm SO_2 inlet concentration was set, while the NO concentration was increased to form a range of N:S ratios. As shown in Figure 15(a), an SO_2 removal efficiency of >98% is attained at any value of N:S ratio when the temperature is 24 °C. This result can be explained considering the relatively high equilibrium solubility of SO_2 in water (Henry's Law) at low temperature.

From Figure 15(a), an increased in N:S ratio results in a higher NO_x scrubbing efficiency, with an approximate increase from 77% to 91% for N:S ratios of 0.5 and 2, respectively. While the overall efficiency increases, the outlet NO_x concentration (Figure 15(b)) increases from 58 to 83 ppm. Experiments were also conducted at an elevated temperature of 202 °C. The results, shown in Figure 15 (c-d), reveal the same trend for N:S ratio, with an increase in N:S from 0.5 to 2 resulting in an efficiency increase from 64% to 81%, corresponding to a 91 ppm and 178 ppm outlet NO_x concentration, respectively. Comparing the 24°C and 202 °C experiments, a 10%. lower NO_x scrubbing efficiency across all N:S ratios was observed at higher gas temperature, which is attributed to a reduced NO oxidation rate occurring at higher temperatures.

A model of the experimental DCC column was developed in ASPEN Plus to simulate the experiments, which included the chemical reaction mechanism outlined in Table 2. The model-predicted outlet concentrations of NO and SO_2 are shown in Figure 15. At low temperatures the NO_x model concentration

shows a 2 – 3% difference in overall scrubbing efficiency. At higher temperatures the model overpredicts NO_x scrubbing, with an overestimation of approximately 5% for all N:S ratios considered. These results indicate the reaction mechanism can predict the outlet concentrations at temperatures up to 200 °C with reasonable accuracy.

Comparing the SO_2 scrubbing efficiency, an almost complete removal of SO_2 (98% / 13 ppm) is observed at low temperature, with 100% scrubbing observed at N:S ratios at 0.5 or greater. At 202 °C, a 90% SO_2 (48 ppm) conversion efficiency is observed, with 100% conversion at N:S ratios of 1 or greater. The SO_2 conversion is limited by SO_2/HSO_3^- equilibrium described by Henry's law, due to the limited solubility of SO_2 at higher temperatures. Therefore, the N:S ratio becomes increasingly important for the removal of SO_2 at elevated temperatures. This is due to the liquid-phase reactions previously discussed (Table 2, Reactions 5 and 6) generating HNO_2 and reacting with HSO_3^-, consuming HSO_3^- and thereby promoting SO_2 dissolution. The model predictions for SO_2 conversion at 24 °C show good agreement, with minor over/under predictions of approximately 1.5%. At 202 °C, the model predicts SO_2 scrubbing well even with no NO, with a predicted SO_2 scrubbing of 90% compared with 91% observed experimentally, and it predicts SO_2 scrubbing accurate at all N:S ratios considered.

Table 5. Operation Conditions Corresponding to Figure 15 and Figure 16

Parameters	
Pressure	15 bar(a)
Temperature	24; 202 °C
Oxygen Concentration	3.1 %
Gas Flowrate	810 SLPM
L:G Ratio	0.97 $kg_{(l)}$:$kg_{(g)}$
Residence Time	130 seconds
NO Inlet Concentration	0 – 960 ppm
SO_2 Inlet Concentration	0 – 960 ppm

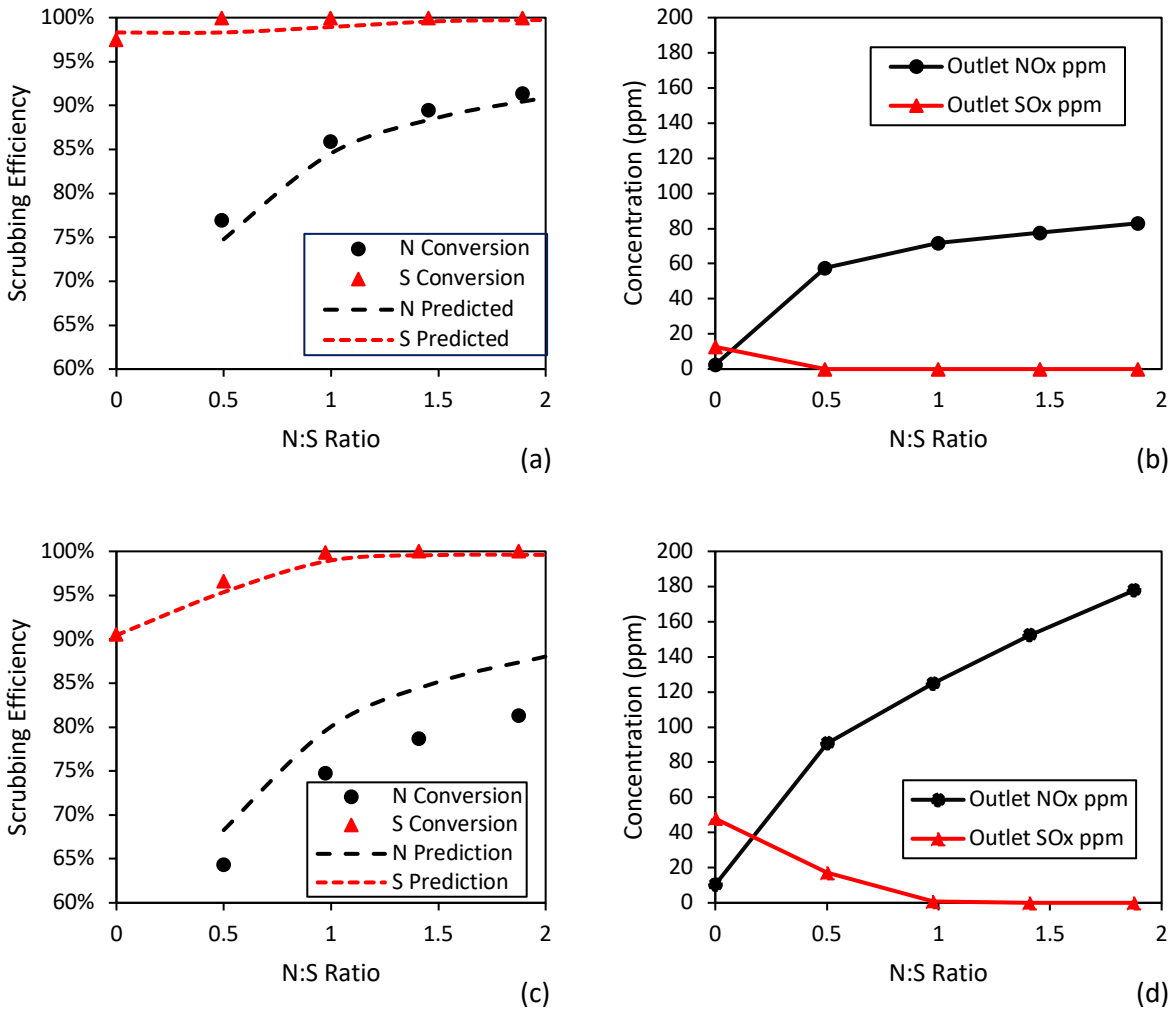

Figure 15. The effect of inlet N:S ratio on scrubbing efficiency and outlet NO_x and SO_2 concentrations at (a-b) 24°C and (c-d) 202°C (inlet SO_2 = 507 ppm and NO_x = 0 – 960 ppm).

d. The Influence of S:N on Conversion

In Figure 16, the S:N ratio was investigated to determine the effect of SO_2 on NO_x capture efficiency. The experiments were operated at the same conditions (Table 5) as Figure 15, with a fixed NO inlet concentration of 495 ppm and a stepwise increase in SO_2 inlet concentration.

In Figure 16(a), at 22°C increasing the S:N ratio results in SO_2 scrubbing of 98.5% at S:N = 0.5 and 100% scrubbing at ratios greater than 1. In Figure 16(c) elevated temperatures (202°C) result in 100% SO_2 scrubbing at all S:N ratios and indicates that an S:N ratio up to 2 does not affect the SO_2/HSO_3^- equilibrium enough to yield SO_2 at the outlet. The model predicts a drop in the SO_2 scrubbing efficiency at 202°C and S:N = 1.5, however this is not observed experimentally.

The NO_x scrubbing efficiency decreases at larger S:N ratios. In Figure 16(a) the NO_x conversion without SO_2 is 87% (62 ppm) and decreases to 85% (78 ppm) at a S:N ratio of 2. In comparison, elevated temperatures cause the decrease in NO_x conversion to becomes more pronounced, with a decrease in conversion from 79% (106 ppm) to 73% (134 ppm) at an S:N ratio of 1.5. In terms of absolute NO_x capture, at 202°C an approximate drop of 10% NO_x scrubbing efficiency is observed, similar to the results observed in Figure 15. The initial model prediction of NO_x scrubbing is similar to the experimental results, however the model does not currently account for the reduced NO_x scrubbing efficiencies at high S:N ratios. This is readily apparent at 202°C, where the scrubbing efficiency is overestimating by 6% at a S:N ratio of 1.5. While this effect has been observed in the literature [24] it has not been strongly investigated due to its low impact at low temperature. The increased effect at elevated temperatures suggests that this assumption could lead to inaccuracies for integrated heat recovery systems. One possible explanation for this trend can be given based on the kinetic rate of Reaction 7 in Table 2. The available literature suggests this rate is negligible; however, if Reaction 7 were more prevalent at elevated temperatures then the outlet SO_2 concentration would decrease, as SO_2 would form SO_3 and disassociate into HSO_4^- directly. Conversely the NO_x outlet concentration would increase due to NO formation throughout the column.

With the conditions outlined in Table 5, a stable outlet pH of approximately 2.4 was observed. These conditions are scale independent and therefore the outlet pH of 2.4 is not expected to vary with increasing column size. The ideal operating pH and practical control of pH is an ongoing question, with a lower pH resulting in faster HSO_3^- consumption and greater SO_2 capture but also resulting in greater N_2O formation. A lower pH may also impact column design and materials, as low pH and high temperatures result in greater corrosion potential.

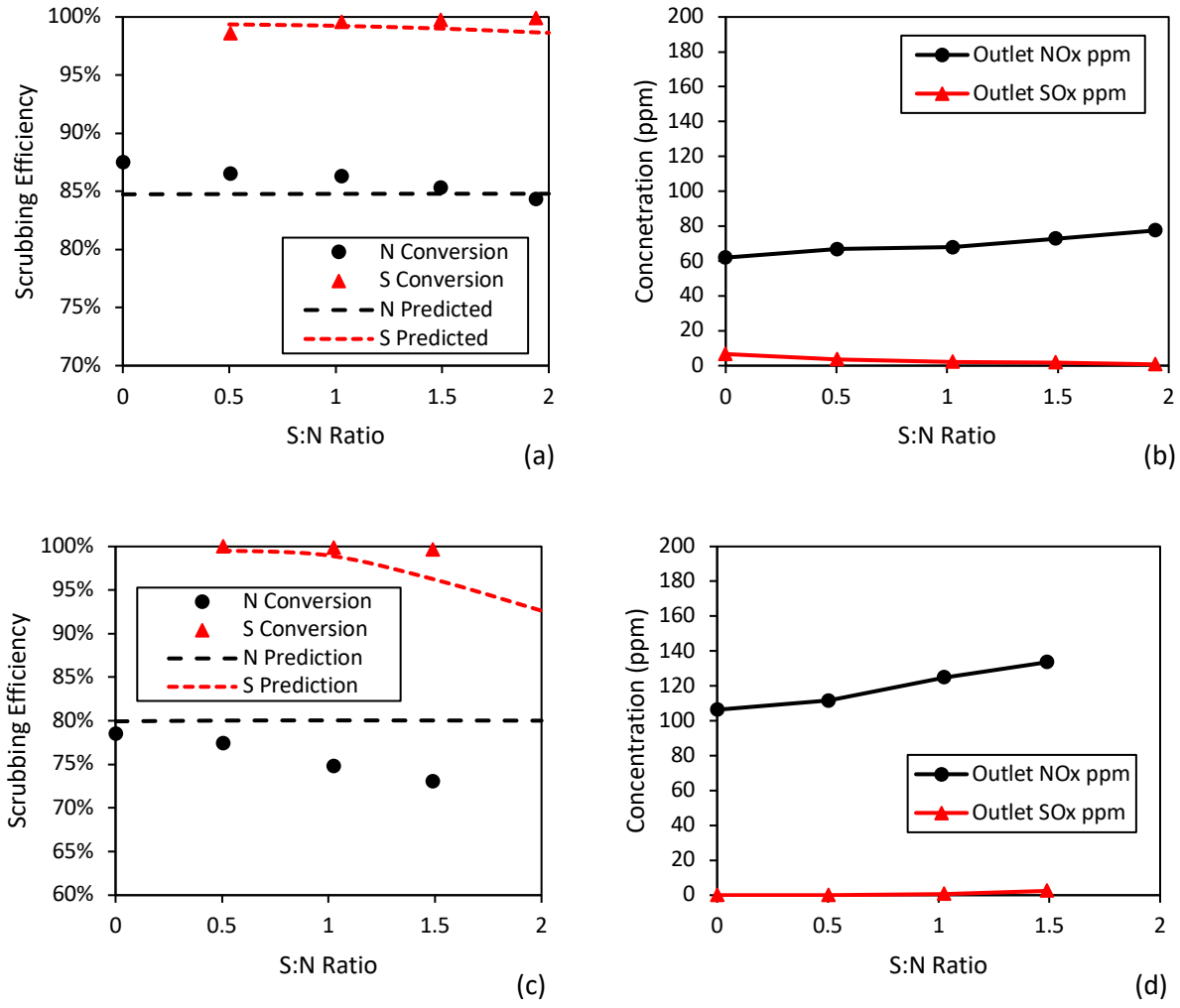

Figure 16. The effect of S:N Ratio on Scrubbing efficiency and outlet NO_x and SO_2 concentrations at (a-b) 24°C and (c-d) 202°C (inlet NO_x = 495 ppm and SO_2 = 0 – 960 ppm)

e. The effect of L:G Ratio

The effect of water flowrate within the DCC has also been investigated. At conditions outlined in Table 6, the liquid to gas (L:G) ratio was varied between 0.6 and 1.6 (kg(l):kg(g)), chosen based on water flowrates required for optimal latent heat recovery in the full-scale DCC (assuming wet flue gas). Figure 17 shows no observable effect of L:G ratio on scrubbing efficiency within this range. At lower L:G ratios the reduced water flow rate increases the HSO_3- concentration in the liquid phase. As a result, Henry's law would cause more SO_2 in the flue gas outlet. For the discussed conditions, the change in water flowrate does not observably affect SO_2 scrubbing within the column. The invariance with L:G ratio shown in Figure 17 implies Henry's law is not limiting SO_2 scrubbing at industry-relevant L:G ratios and SO_2 concentrations.

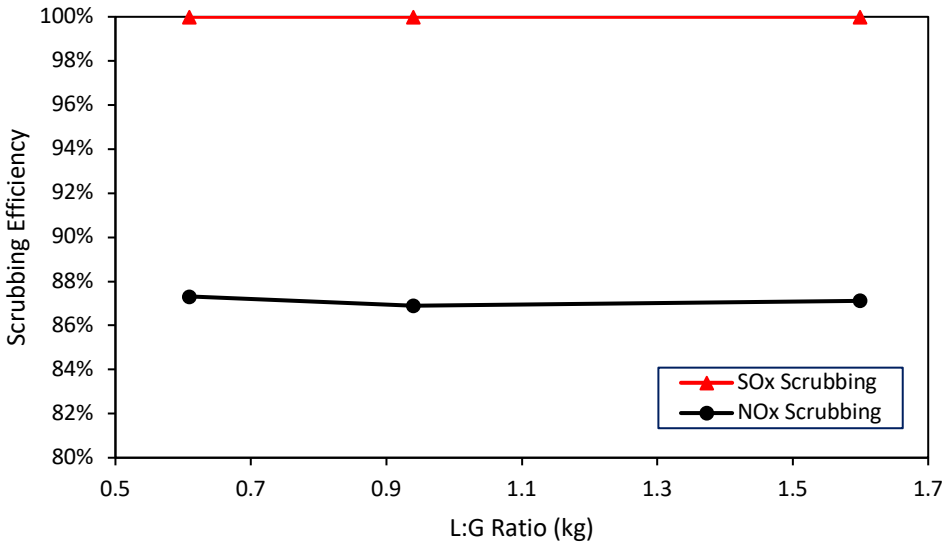

Figure 17. The effect of L:G Ratio on Scrubbing Efficiency at 22°C.

Table 6. Operation Conditions Corresponding to Figure 17

Parameters	
Pressure	15 bar(a)
Temperature	23 °C
Gas Flowrate	807 SLPM
Oxygen Concentration	1.1 %
L:G Ratio	0.61 – 1.6 $kg_{(l)}$:$kg_{(g)}$
Residence Time	130 seconds
NO Inlet Concentration	540 ppm
SO_2 Inlet Concentration	506 ppm

f. A comparison with currently existing models

Recently, Tumsa et al. [8] mathematically investigated a full-scale pressurized oxy-combustion DCC column and determined the scrubbing efficiency over a range of different conditions (Table 7). While not directly comparable, the trends can be compared to the current experimental results.

Table 7. Conditions modeled in Tumsa et al. [8]

Conditions	
Pressure	5-30 bar
L:G	3 $kg_{(l)}$: $kg_{(g)}$
Gas Flowrate	120 kg/s
Gas Inlet Temperature	20 – 150 °C
Residence Time	73 seconds
Gas Composition	
CO_2	87.56 %
O_2	2.7 %
H_2O	9.0 %
SO_2	0.2 %
NO	0.04 %
N_2	0.4 %

Tumsa et al. observed that an increase in temperature from 20°C to 150°C reduced NO_x capture by 2% (70 to 68%) whereas the experimental results obtained in this work showed a 10% drop in NO_x capture between 22°C and 202°C (83 to 73%). In both cases the SO_2 capture was 100%. In general, our experimental results show greater NO_x scrubbing than anticipated in Tumsa. This may be due to several factors but is most likely due to the longer residence times in the experimental system.

At an L:G ratio less than 1.5 $kg_{(l)}$:$kg_{(g)}$ Tumsa showed a much lower SO_2 scrubbing efficiency, and below 1 the NO_x scrubbing showed minor decreases. In contrast with our experimental findings, an L:G ratio less than 1 $kg_{(l)}$:$kg_{(g)}$ showed no change in SO_2 scrubbing efficiency, with conversion still at 100%. The reason for this discrepancy is attributed to the higher SO_2 concentration in Tumsa. Tumsa used 2000 ppm, resulting in higher HSO_3^- concentrations and affecting the SO_2/HSO_3^- equilibrium. Additionally, the liquid chemistry currently available in literature differs from the results experimentally outlined in our previous sections, and this would affect the accuracy of Tumsa's predictions for HSO_3^- consumption.

5.3 Conclusions

The operation of an experimental Direct Contact Column (DCC) has provided a range of experimental data at a scale and temperature representative of a scrubbing column with integrated heat recovery. In the majority of experiments, the SO_2 capture approached 100%, making the NO_x capture the primary metric of capture efficiency. A residence time of 95 seconds at 11 bar showed the highest NO_x capture efficiency at the smallest time experimentally attainable. An inflection point was observed at an oxygen partial pressure of 0.1 bar, at which point the effect of O_2 partial pressure on NO_x capture rate showed diminishing returns. Investigations of S:N and N:S ratios showed a minor decrease in NO_x conversion with larger S:N ratios, while SO_2 conversion stayed close to 100%. The NO capture increased with N:S ratios, however the outlet NO concentration also increased. The N:S ratios also display a non-100% SO_2 capture at low ratios, with a ratio of 1 resulting in 100% capture. At higher temperatures (202°C inlet gas temperature), the trends remain consistent, however the total NO_x scrubbing efficiency was reduced by approximately 10% and this

is attributed to a reduced NO oxidation rate. Based on the operating conditions and water flowrates relevant for heat recovery, no effect of L:G ratio was observed. The combination of higher temperature and low N:S ratio showed a significant amount of SO_2 present in the gas outlet (10%) and highlights the necessity of NO_x in the flue gas for sulfur scrubbing when latent heat recovery is utilized.

6. Full-scale Modeling of the DCC

A full-scale Direct Contact Column was modeled in Aspen Plus (V9) to estimate the dimensions of the column for a 550 MWe SPOC power plant. As described in Section 5.1, the column was modeled as a rate-based reactive absorption column using the RadFrac unit with ELECNRTL as the property method. The reactions used for the simulation are described in Table 2, with the equilibrium reactions handled directly in Aspen Plus. For the kinetic reactions, Reactions 1 and 7 were supplied through a kinetic subroutine written separately and kinetic parameters for Reactions 5 and 6 were provided in the form of a power-law expression in Aspen Plus. The packing material for gas-liquid contact was considered to be Raschig metal rings. The cooling water flow rate required for recovery of latent and sensible heat from the flue gas was based on the outlet flue gas moisture concentration. The target moisture concentration at the outlet of the flue gas was kept to less than 1.5% v/v. The inlet flue gas composition of relevant species is presented in Table 8.

Table 8. Inlet Flue Gas Composition

Inlet Flue gas composition	
O_2	3 %
H_2O	39 %
SO_2	700 ppm
SO_3	250 ppm
NO	700 ppm
NO_2	250 ppm

Two approaches were used for sizing the diameter and height of the column:

a) Single Column: The overall process flow diagram of the DCC is presented in Figure 18. The column diameter was sized based on an 80% approach to flooding velocity, which is in the typical range of operating conditions for scrubbing columns. The height of the column was determined based on the residence time required for reducing the SOx concentration in the flue gas to less than 15 ppm. The calculations predict that a column operating at an 80% approach to the flooding

velocity will have a diameter of 5 meters and require 80.4 seconds to reduce the SOx concentration to less than 15 ppm. Based on this, the height of the column was calculated to be 60 meters. Almost 76% of NOx was removed in this process.

b) Two Columns: The overall process flow diagram of the DCC is presented in Figure 19. Because a column with a diameter of 5 meters is difficult to manufacture and transport, this design could lead to unnecessary capital and transportation costs. Consequently, a two-column system, with each column being 4 meters in diameter was considered. This size was chosen as it is suitable for factory fabrication and easy transport to the site. In this approach, the flow rate of the gas was split equally into the two parallel columns and all other target conditions for the sizing were kept consistent. The approach to flooding velocity was found to be 71%, which is in the range of optimal operating conditions. The results indicate that the 4-meter columns require 77.1 seconds to reduce the concentration of SOx to 15 ppm. Hence, the height required is almost 45 meters for each column. In the process, 72% of the NOx was also removed. The small difference in NOx removal between the two approaches (one single column versus two parallel columns) is because of the change in residence time and the temperature profile inside the column, which affects the reaction rates.

A summary of the results is presented in Table 9. Based on these findings, either of the above approaches can be used for designing the Direct Contact Column(s). The final choice will depend on capital and transportation costs.

Table 9. Summary of the results of full-scale DCC modeling

Outlet Gas	Single Column	Double Column
H_2O Concentration	< 1.5% v/v	< 1.5% v/v
SOx Removal	> 99%	> 99%
NOx Removal	76%	72%
Column Design Specification		
Diameter	5 m	4 m
Height	60 m	45 m
Residence Time	80.4 s	77.1 s

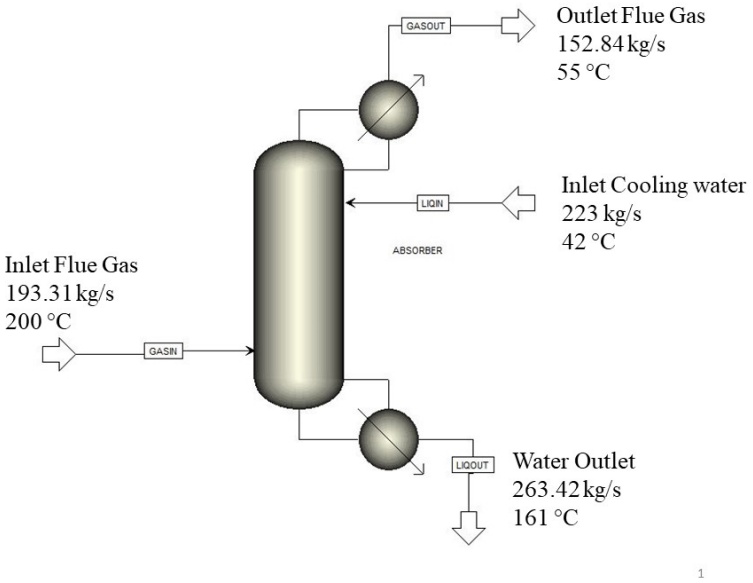

Figure 18. The process flow diagram of the Direct Contact Column for a 550 MWe SPOC power plant.

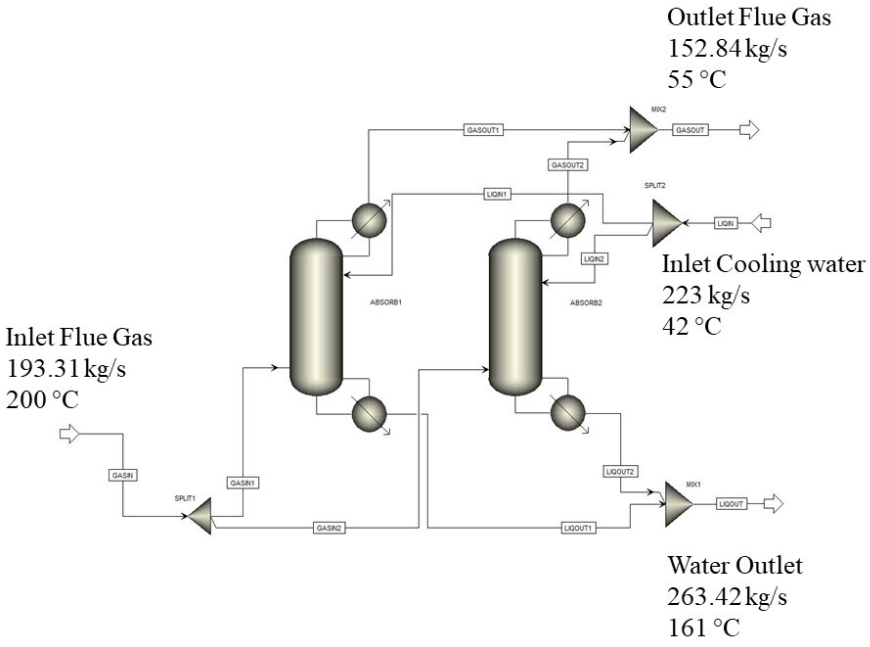

Figure 19. The process flow diagram of two parallel Direct Contact Columns for a 550 MWe SPOC power plant.

7. Recommendations for Future Work

The results of this study indicate that the DCC technology can be used effectively in the Staged Pressurized Oxy-Combustion process to capture the latent heat from the flue gas moisture while simultaneously scrubbing SOx and NOx. While additional work would be valuable to allow for optimization of full-scale designs, our study did not identify any barriers or significate risks associated with the technology. In terms of recommendations for future work, we propose the following to enhance to performance of the DCC with respect to plant efficiency, scrubbing efficiency and the liquid phase products:

1) The investigation into scrubbing has shown that NO oxidation is the primary driver for nitrogen capture. As such the investigation into the feasibility of oxidants or catalysts for high temperature NO oxidation would be valuable to yield a single, integrated DCC column.
2) Since the goal of the pressurized DCC for the SPOC process is to increase plant efficiency through latent heat capture, the DCC operates at higher temperature than in previous studies of IPR, where the flue gas from atmospheric pressure oxy-combustion was compressed. The results of our study have shown that higher temperature reduces SO_2 scrubbing efficiency and that the nitrogen and sulfur interactions in the aqueous phase are integral to the consumption of HSO_3^-, which is essential to ensure complete SO_2 scrubbing. Thus, the chemistry and stability associated with the HADS complex should be better understood, particularly with respect to decomposition at higher temperature. The chemistry of the HADS complex also has a significant effect on the formation of N_2O in the outlet stream, further justifying the need for additional studies.
3) For N:S ratios greater than unity, SO_2 scrubbing is quite effective. However, for conditions where NOx formation is low, the scrubbing efficiency falls off. While the N:S ratio for the SPOC process is expected to be greater than unity, other approaches to pressurized combustion that may operate at lower combustion temperature, e.g., Pressurized Flameless Combustion, could have low N:S ratios. Thus, alternative methods of enhancing HSO_3^- consumption should be explored. For example, investigating potential additives to promote high temperature, stable complex formation

to increase HSO_3^- consumption rate, and therefore scrubbing efficiency under low N:S ratio conditions, should be investigated.

4) Residual fly ash coming off of the particle removal system could affect the Ph in the DCC and possibly the liquid phase chemistry, thus, the potential effects of fly ash contaminants should be investigated.
5) Lastly, while this work has shown that the SPOC DCC system is effective at accomplishing the proposed objectives, further studies are needed to optimize the process in terms of plant efficiency and scrubbing efficiency. In particular, future studies should focus on the effects of residence time and outlet gas and water temperatures to ensure that the DCC performance can be optimized.

Appendix A - References

[1] S. Kobayashi, L. E. Bool, in: *Oxy-fuel combustion for power generation and carbon dioxide capture*, L. Zheng, (Ed.) Woodhead Publishing: 2011.

[2] R. Axelbaum, F. Xia, A. Gopan, B. Kumfer, Staged High-Pressure Oxy-Combustion Technology: Development and Scale-Up, Phase I Topical Report, 2014.

[3] A. Gopan, B. M. Kumfer, R. L. Axelbaum, International Journal of Greenhouse Gas Control 39 (2015) 390-396.

[4] A. Gopan, B. M. Kumfer, J. Phillips, D. Thimsen, R. Smith, R. L. Axelbaum, Applied Energy 125 (2014) 179-188.

[5] F. Xia, Z. Yang, A. Adeosun, A. Gopan, B. M. Kumfer, R. L. Axelbaum, Fuel 181 (2016) 1170-1178.

[6] F. Xia, Z. Yang, A. Adeosun, B. M. Kumfer, R. L. Axelbaum, Fuel 172 (2016) 81-88.

[7] H. Hagi, M. Nemer, Y. Le Moullec, C. Bouallou, Energy Procedia 63 (2014) 431-439.

[8] T. Z. Tumsa, S. H. Lee, F. Normann, K. Andersson, S. Ajdari, W. Yang, Chemical Engineering Research and Design 131 (2018) 626-634.

[9] V. White, A. Wright, S. Tappe, J. Yan, Energy Procedia 37 (2013) 1490-1499.

[10] R. Stanger, T. Ting, C. Spero, T. Wall, International Journal of Greenhouse Gas Control 41 (2015) 50-59.

[11] X. Li, Q. Huang, C. Luo, Z. Zhang, Y. Xu, L. Zhang, C. Zheng, Fuel 234 (2018) 1285-1292.

[12] F. Raschig, Z. Angew. Chem 17 (1904) 1777-1785.

[13] F. Seel, E. Degener, Zeitschrift für anorganische und allgemeine Chemie 284 (1-3) (1956) 101-130.

[14] S. Yamamoto, T. Kaneda, Nippon Kagaku Zasshi 80 (1098) (1959) 0.

[15] S. Oblath, S. Markowitz, T. Novakov, S. Chang, The Journal of Physical Chemistry 85 (8) (1981) 1017-1021.

[16] S. M. Pétrissans, A. Pétrissans, A. Zoulalian, Chemical Engineering and Processing: Process Intensification 44 (10) (2005) 1075-1081.

[17] S. Chang, D. Littlejohn, N. Lin, Kinetics of reactions in a wet flue gas simultaneous desulfurization and denitrification system, Symposium on Advances in Flue Gas Desul furi zat ion, ACS, Atlanta, Georgia (March 30-April 3, 19'81), 1982.

[18] F. Normann, E. Jansson, T. Petersson, K. Andersson, International Journal of Greenhouse Gas Control 12 (2013) 26-34.

[19] S. Ajdari, F. Normann, K. Andersson, F. Johnsson, Industrial & Engineering Chemistry Research 55 (19) (2016) 5514-5525.

[20] S. Ajdari, F. Normann, K. Andersson, F. Johnsson, Industrial & Engineering Chemistry Research 54 (4) (2015) 1216-1227.

[21] R. L. Axelbaum, Integrated Flue Gas Purification and Latent Heat Recovery for Pressurized Oxy-Combustion, 2017 NETL CO2 Capture Technology Project Review Meeting Aug. 25 2017, 2017.

[22] M. Pires, M. J. Rossi, International journal of chemical kinetics 29 (12) (1997) 869-891.

[23] S. Oblath, S. Markowitz, T. Novakov, S. Chang, The Journal of Physical Chemistry 86 (25) (1982) 4853-4857.

[24] V. White, A. Wright, S. Tappe, J. Yan, Energy Procedia to appear (2013).

[25] H. Tsukahara, T. Ishida, M. Mayumi, Nitric Oxide 3 (3) (1999) 191-198.

[26] C. Iloeje, R. Field, A. F. Ghoniem, Fuel 160 (2015) 178-188.

[27] K. Skalska, J. S. Miller, S. Ledakowicz, Chemical Papers 64 (2) (2010) 269-272.

[28] Q. Cheng, D. Liu, J. Chen, J. Jin, W. Li, S. Yu, Chinese Journal of Chemical Engineering (2018).

[29] J. Greig, P. Hall, Transactions of the Faraday Society 62 (1966) 652-658.

[30] J. Greig, P. Hall, Transactions of the Faraday Society 63 (1967) 655-661.

[31] M. Morrison, R. Rinker, W. Corcoran, Industrial & Engineering Chemistry Fundamentals 5 (2) (1966) 175-181.

Appendix B – List of Presentations

BM. Kumfer, D Stokie, P Verma, Y-S Jun, G Yablonsky, A K Suresh, RL Axelbaum, "Integrated Flue Gas Purification for Staged Pressurized Oxy-Combustion" International Pittsburgh Coal Conference, Xuzhou, China, Oct 15-18, 2018.

Yablonsky G., Stokie D., Kumfer B, Verma P, Min Y, Zhu Y, Jun Y, Suresh A, Axelbaum R "The Kinetics of Flue Gas Purification for Pressurized Oxy-Combustion" XXIII International Conference on Chemical Reactors CHEMREACTOR-23 Ghent, Belgium, November 5-9, 2018.

D. Stokie, B. Kumfer, P. Verma, Y. Min, Y. Zhu, Y.-S. Jun, G. Yablonsky, A.K. Suresh, R. L. Axelbaum, "Integrated Flue Gas Purification for Staged Pressurized Oxy-Combustion" Clearwater Clean Energy Conference, Clearwater, FL, June 3-7, 2018.

R.L. Axelbaum, Integrated Flue Gas Purification and Latent Heat Recovery for Pressurized Oxy-combustion. NETL CO2 Capture Technology Project Review Meeting, Pittsburgh, PA, Aug. 25, 2017.

Y. Min, Y. Sun, Y.-S. Jun, G. Yablonsky, B. Kumfer, R. Axelbaum. "Experimental study of SOx and NOx removal from oxy-combustion flue gas under high pressure" Clearwater Clean Energy Conference, Clearwater, FL, June 11-17, 2017.

R.L. Axelbaum, Staged High Pressure Oxy-combustion Technology: Development and Scale-Up, Phase 2. NETL CO2 Capture Technology Project Review Meeting, Pittsburgh, PA, Aug. 12, 2016. (presented by Ben Kumfer)

R.L. Axelbaum, Integrated Flue Gas Purification and Latent Heat Recovery for Pressurized Oxy-combustion. NETL CO2 Capture Technology Project Review Meeting, Pittsburgh, PA, Aug. 12, 2016. (presented by Ben Kumfer)

R.L. Axelbaum, Development of staged pressurized oxy-combustion. 5th Oxyfuel Combustion Research Network Meeting. Wuhan, China. Oct. 27-30, 2015.